

## On the Use of Earth Radiation Budget Statistics for Studies of Clouds and Climate<sup>1</sup>

DENNIS L. HARTMANN AND DAVID A. SHORT

*Department of Atmospheric Sciences, University of Washington, Seattle 98195*

(Manuscript received 17 October 1979, in final form 28 February 1980)

### ABSTRACT

Daily observations of albedo and outgoing terrestrial radiation derived from NOAA Scanning Radiometer measurements are used to relate cloudiness variations to regional features of the general circulation and to estimate the relative importance of the albedo and infrared effects of clouds on the net radiation balance of the earth on a regional basis. The results indicate that there are clear relationships between the variability in outgoing IR and features of the atmospheric circulation, which appear to be linked to changes in cloudiness. A method requiring only measurements of planetary albedo and total outgoing IR is devised to evaluate the relative importance of the albedo and IR effects of the current distribution of cloud for the net radiation balance of the earth. The results obtained from this method suggest that globally the effect on the radiation balance of the high albedo of clouds is two or more times greater than the effect of clouds in reducing outgoing IR, so that an increase in the fractional area of the current distribution of cloud would tend to cool the earth. In addition, very large geographical variations in the radiative effects of cloud are displayed and related to circulation features.

### 1. Introduction

During the past two decades satelliteborne instruments have been developed and deployed to measure the earth's radiation budget (ERB) at the top of the atmosphere. The ERB data from past satellites have improved our understanding of the global climate system of the earth (e.g., Winston, 1969; Vonder Haar and Suomi, 1971; Raschke *et al.*, 1973; Jacobowitz *et al.*, 1979) and future ERB measurement systems promise to add much more to our understanding of global, regional and diurnal heat budgets. The largest day-to-day variations in the earth's planetary albedo and outgoing thermal radiation are caused by variations in clouds. Although clouds play an important role in determining the present climate (e.g., Manabe and Wetherald, 1967), and could potentially be very important in determining the sensitivity of climate, our understanding of the maintenance of the current cloud climatology is sadly deficient. In addition, there remains some uncertainty even concerning what the net radiative effect of cloud is, particularly on a regional basis. Since clouds have such a strong signature in ERB measurements, and the radiation balance at the top of the atmosphere is so central to the maintenance of climate, one can hope to

learn something about the relationship between clouds and climate by studying ERB data.

In this paper we experiment with methods by which ERB data can be used to enhance our knowledge of how clouds affect the radiation balance and how the circulation patterns are related to the type of cloud present in particular regions. We are concerned with two main objectives. The first of these is to demonstrate how the statistics of the ERB measurements of planetary albedo and outgoing terrestrial radiation are mutually related to cloudiness and to the atmospheric general circulation. These correspondences suggest comparing higher order statistics of ERB measurements with similar statistics derived from general circulation model experiments. In this way it may be possible to determine whether the cloud prediction schemes being inserted into some general circulation models are likely to be adequate for climate sensitivity studies.

The second application of the ERB data which we undertake is to evaluate the net radiative effect of the current distribution of cloud on the heat balance of the earth. This is accomplished with ERB measurements of planetary albedo and outgoing terrestrial radiation alone and without auxiliary measurements of fractional area coverage of cloud or assumptions about cloud height or albedo. The method employed also allows the net radiative effect of cloudiness to be presented in map form for individual seasons.

<sup>1</sup> Contribution No. 529, Department of Atmospheric Sciences, University of Washington.

## 2. Data

The data employed in this study consist of two seasons of NOAA Scanning Radiometer observations of albedo ( $\alpha$ ) and total outgoing terrestrial radiation ( $F$ ). The total reflected solar radiation was determined from observations in the visible (0.5–0.7  $\mu\text{m}$ ) portion of the spectrum and the total outgoing terrestrial radiation (hereafter outgoing IR) was determined from observations in the atmospheric window (10.5–12.5  $\mu\text{m}$ ). A discussion of the regression approach used to derive the total IR flux from the window measurements and further description of these particular data can be found in Gruber and Winston (1978). In the determination of the regression relationship the data of Roberts *et al.* (1976) have been used to take into account the continuum absorption by water vapor in the 8–12  $\mu\text{m}$  region.

In applying these data for studies of climate several uncertainties associated with currently available ERB data in general and with NOAA Scanning Radiometer data in particular must be borne in mind. These uncertainties arise from two general classes of problems with determining the radiation balance at the top of the atmosphere from satellite radiance observations. The first class of problems is associated with the conversion of a satellite instrument reading to an exitance at the top of the atmosphere at a particular point and time. In the case of the data employed here the total outgoing IR and reflected solar radiation are inferred indirectly from measurements in limited portions of the IR and solar spectra. Although the regression model used to convert narrow-band measurements into total exitance describes well the relation between computed narrow-band and total exitances, it is still possible that some misrepresentation of the contrast between different fields of view may be introduced by this procedure. In addition, isotropic reflection is assumed in order to convert measurements made by the scanning instrument into hemispherically integrated reflected solar flux at the top of the atmosphere. This assumption undoubtedly introduces some error.

The second set of problems has to do with sampling in space and time in such a manner as to obtain representative estimates of the true earth radiation budget. One of the most serious sampling biases is that the sun-synchronous polar-orbiting satellites measure reflected solar radiation at only one local time and outgoing IR at only two local times. It is known that the albedo of a particular field of view changes with zenith angle and that the cloudiness and surface temperature vary with the time of day in most regions.

Even with all of these hazards NOAA Scanning Radiometer data have provided many insights into

the earth's radiation budget. Moreover, there are now more than four years of data from this instrument which are available in convenient form. These data represent a considerable resource which should be completely, if carefully, exploited. In this paper we explore a few of the ways in which these data can be used to gain insight into the earth's climate and to provide needed verification for climate models.

The data we will discuss were taken from the sun-synchronous polar orbit of the NOAA 4 satellite with equatorial crossings at 0900 and 2100 local time. We have used only the 0900 data. The variations in outgoing IR between 0900 and 2100 present in this data are substantial and are discussed in Short and Wallace (1980), who showed that they are caused by diurnal variations in both surface temperature and cloudiness. A full assessment of the importance of these variations for the earth's radiation budget will have to await observations of the complete diurnal cycle. The data were obtained from NOAA through NCAR on daily  $2.5^\circ \times 2.5^\circ$  latitude-longitude grids. In this preliminary study we have used only the data at  $5^\circ \times 5^\circ$  latitude-longitude intersections to construct our maps. Some of the data on the grids provided to us were identified as interpolated values. We have not used those. The particular seasons for which we will present results are June–August 1975 and December 1975–February 1976.

## 3. Seasonal means and standard deviations

Monthly, seasonal or annual mean maps of satellite observations of albedo, outgoing IR and net radiation have been shown by a number of previous authors (e.g., Winston, 1967; Vonder Haar and Suomi, 1971; Raschke *et al.*, 1973).

Net radiation is defined as

$$R_{\text{net}} = Q(1 - \alpha) - F, \quad (1)$$

where  $Q$  is the available solar radiation,  $\alpha$  the planetary albedo and  $F$  the outgoing terrestrial flux. Maps of  $F$ ,  $\alpha$  and  $R_{\text{net}}$  for the two seasons we will discuss are shown for reference in Figs. 1–3. These maps are similar to maps displayed in the papers referenced above and reveal many interesting features related to the circulation patterns and cloudiness. The major tropical precipitation zones over South and Central America, Africa and Indonesia, as well as the ITCZ are characterized by low outgoing IR and high albedo, which results from the presence of persistent tall cumulus clouds. The seasonal movement of these features is apparent. Regions of high albedo and high outgoing IR over subtropical oceans west of the continents reflect the persistent low-level stratiform cloud associated with subsidence over cold ocean currents.

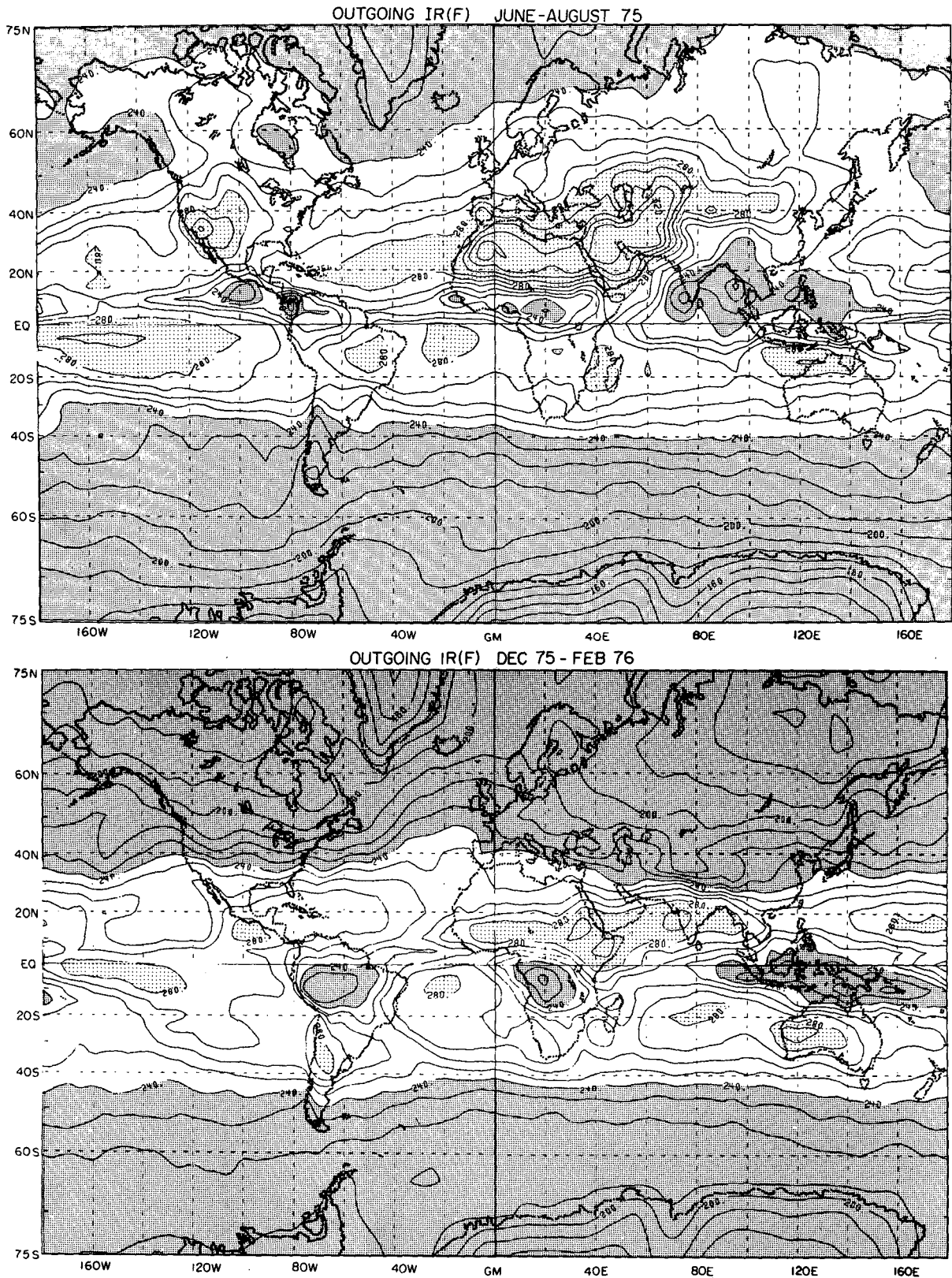


FIG. 1. Mean outgoing IR for two seasons mapped on a Mercator projection. Contour interval is every 10  $W m^{-2}$  with values greater than 280  $W m^{-2}$  stippled and values less than 240  $W m^{-2}$  shaded.

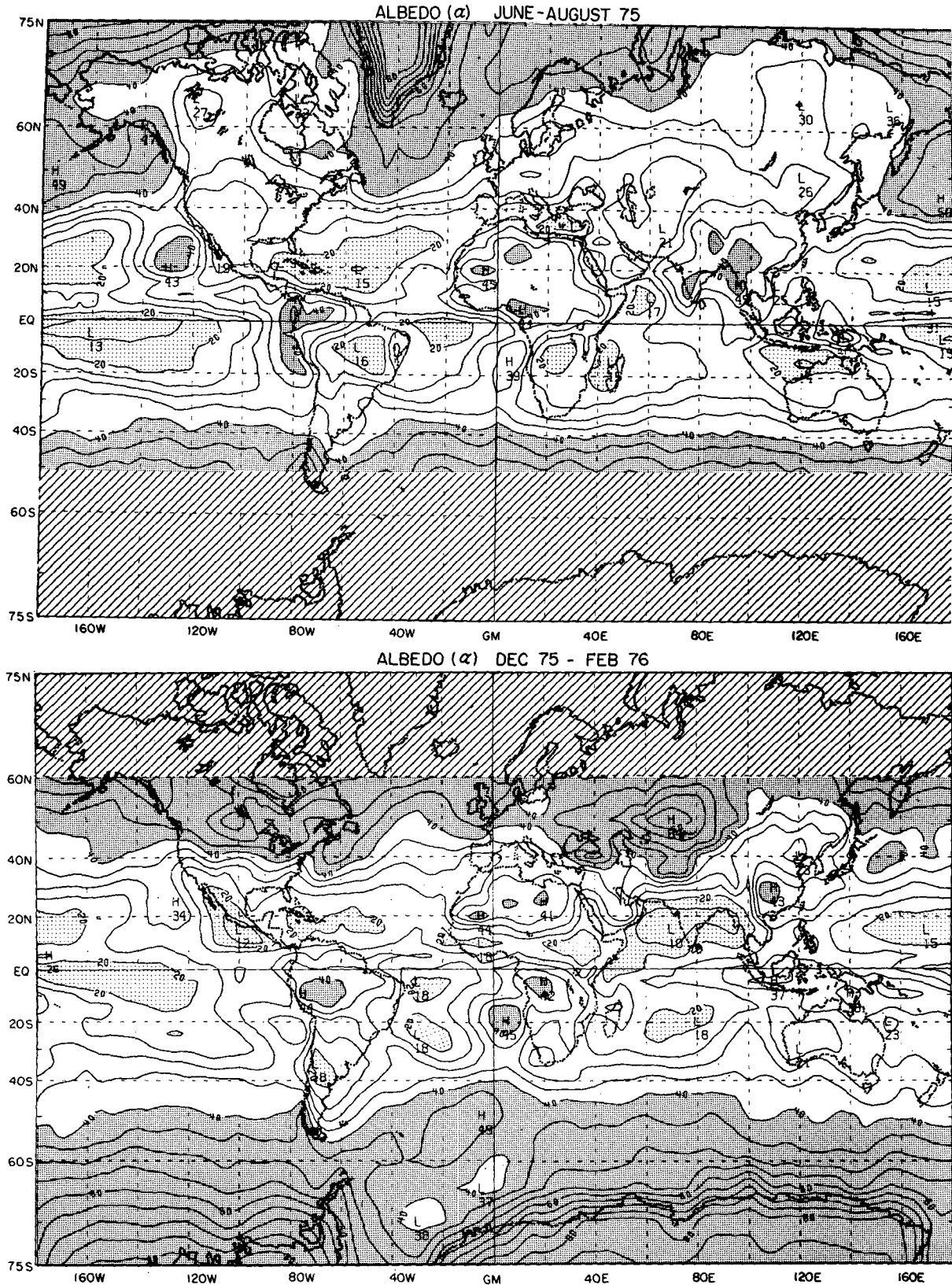


FIG. 2. Mean albedo (percent) for two seasons. Contour interval is every 5% with values less than 20 stippled and values greater than 40 shaded. Very sparse or unreliable data are indicated by cross hatching.

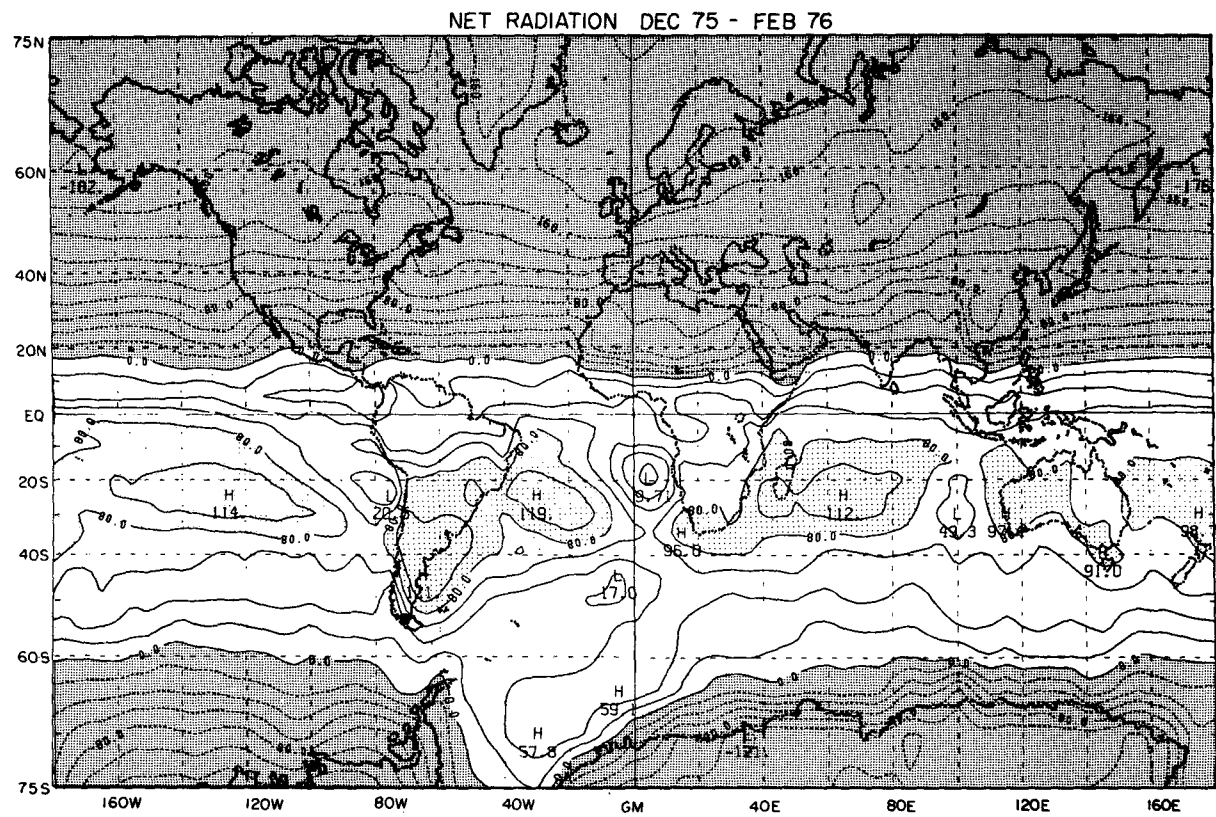
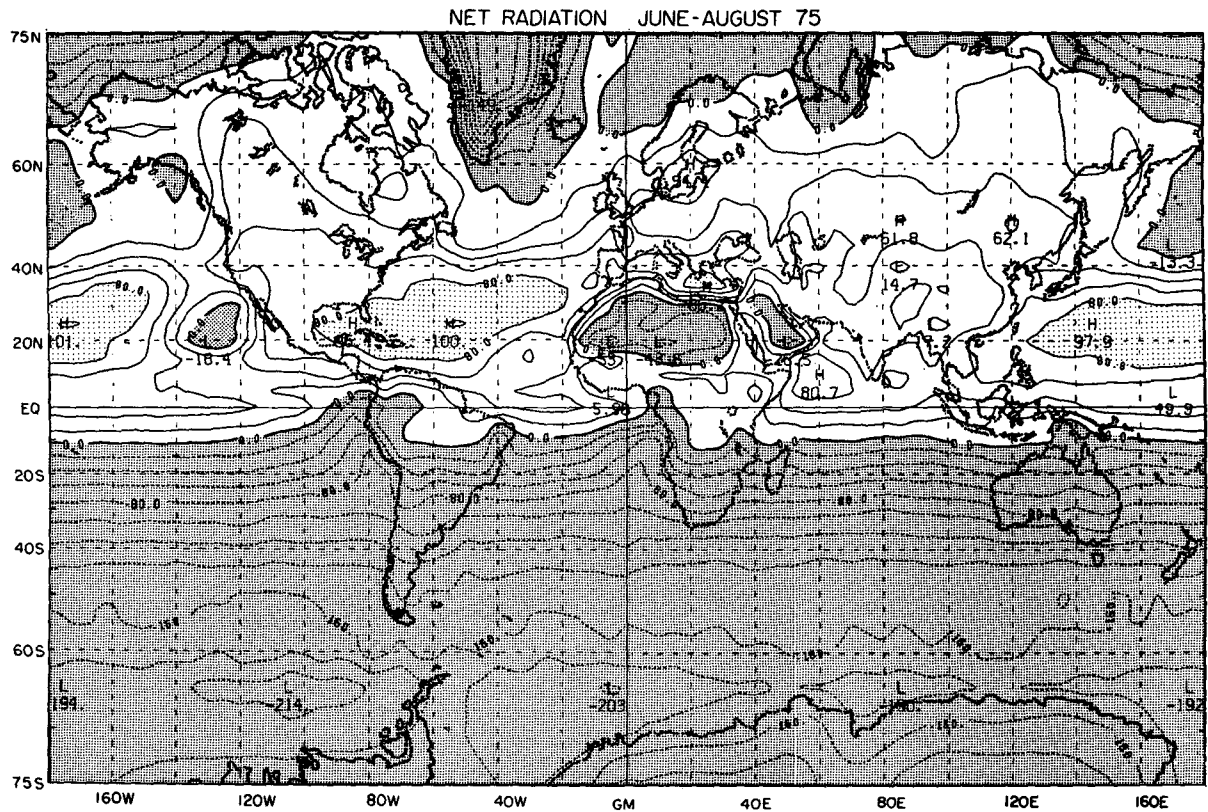


FIG. 3. Net radiation  $R_{net}$  for two seasons. Contour interval is every  $20 \text{ W m}^{-2}$  with values greater than  $80 \text{ W m}^{-2}$  stippled and values less than zero shaded.

The subtropical dry zones are characterized by high outgoing IR with low albedos over the oceans and high albedos over the deserts. Both the deserts and the regions of persistent stratus are areas where the net radiative imbalance can be small or negative in the tropics. The major ice sheets are regions of large negative net radiation due to the high albedo of snow and ice. The contrast in net radiation at a given latitude between Greenland and North America during summer is especially striking. The net radiation over North America during summer is also greater than that over the oceans at latitudes poleward of about 40°N, because of the high frequency of low clouds over the oceans at these latitudes.

In addition to the seasonal means, the standard deviations derived from day-to-day variations of albedo and outgoing IR at various locations also show interesting features related to the atmospheric circulation. Fig. 4 shows the standard deviation of outgoing IR,  $\sigma(F)$ , for two seasons. Where this statistic is large it suggests that high cloud tops are common and where it is small it indicates that high cloud tops are relatively rare. The effect of air temperature and humidity changes on outgoing IR are generally small compared to the effects of middle and high cloudiness. The low-cloud regimes and the relatively cloudless areas appear as regions of low  $\sigma(F)$  in Fig. 4. These are very apparent over the subtropical eastern oceans in both hemispheres. High-latitude oceans are also regions of relatively low cloud and hence low  $\sigma(F)$ .

The major rainfall zones as indicated in the discussion of Figs. 1 and 2 are regions of high  $\sigma(F)$  and hence, as expected, regions where tall clouds are very often present. The boundaries between the convection zones and the drier low-cloud regimes are clearly indicated by very sharp gradients in  $\sigma(F)$ . The position of the Intertropical Convergence Zone (ITCZ) is also clearly shown in the standard deviation of outgoing IR.

The major storm tracks can be identified with regions of high  $\sigma(F)$  which extend eastward and poleward into the midlatitudes of both hemispheres. The well known storm tracks of the Northern Hemisphere which exist to the east of the Asian and North American continents and have been extensively studied using conventional upper air observations (e.g. Lau, 1979a,b) are apparent in Fig. 4 during both seasons. Also shown in Fig. 4 are the storm tracks of the Southern Hemisphere which appear over the southwest Pacific Ocean and east of South America and southern Africa. During Southern Hemisphere winter these storm tracks join into a more or less continuous band of high  $\sigma(F)$  in midlatitudes, whereas in summer they are separated by low-cloud regimes. The orientation of

some regions of high  $\sigma(F)$  is consistent with the predictions of the dynamical model of Grose and Hoskins (1979). For example, one might speculate that the V-shaped pattern of high  $\sigma(F)$  extending northeast and southeast from the Amazon basin during summer is indicative of wave energy propagating away from a region of intense excitation due to latent heat release and topography.

The region of high variability of  $F$  located at about 40°N, 100°E during summer corresponds to an axis of maximum westerly winds at 200–300 mb (Ramage and Raman, 1972). This semi-arid high plateau area experiences a summer maximum of rainfall with frequent high-level clouds and thunderstorms whose precipitation often evaporates before reaching the ground (Arakawa, 1969). The generally high values of  $\sigma(F)$  over North America and Eurasia at high latitudes during summer indicates deeper convection over the continents, which is consistent with the generally warmer surface temperatures over land than over ocean due to strong solar heating of the land surface.

Another interesting feature of the  $\sigma(F)$  distribution appears in the eastern North Pacific during winter. A broad band of large variability in outgoing IR centered at about 10°N and associated with the ITCZ is directly connected to the maximum in  $\sigma(F)$  associated with the North Pacific storm track. Direct connections between tropical and mid-latitude cloud patterns have been described previously by Erickson and Winston (1972). The northern winter of 1975–76 was one during which a large negative 700 mb geopotential anomaly was present over the central North Pacific and a positive geopotential anomaly persisted over the west coast of North America (Wagner, 1976; Taubensee, 1976). These height anomalies may be related to the particular pattern of convective activity in the North Pacific suggested by Fig. 4.

The standard deviation of planetary albedo,  $\sigma(\alpha)$ , over two seasons is shown in Fig. 5. While this statistic does not distinguish between high and low clouds, it distinguishes very well between low-cloud regimes and relatively cloudless areas over the oceans. The dry zones over the oceans which are characterized by low albedos and very little cloud are distinguished by very low values of  $\sigma(\alpha)$  as are the deserts and ice-covered areas where the contrast between the planetary albedo under cloudy and clear conditions is very small.

#### 4. Linear correlation between albedo and outgoing IR

In the previous section we discussed the geographical distributions of the seasonal mean and the standard deviations over the season of albedo and outgoing IR. It was assumed that the temporal variability in these two quantities results primarily

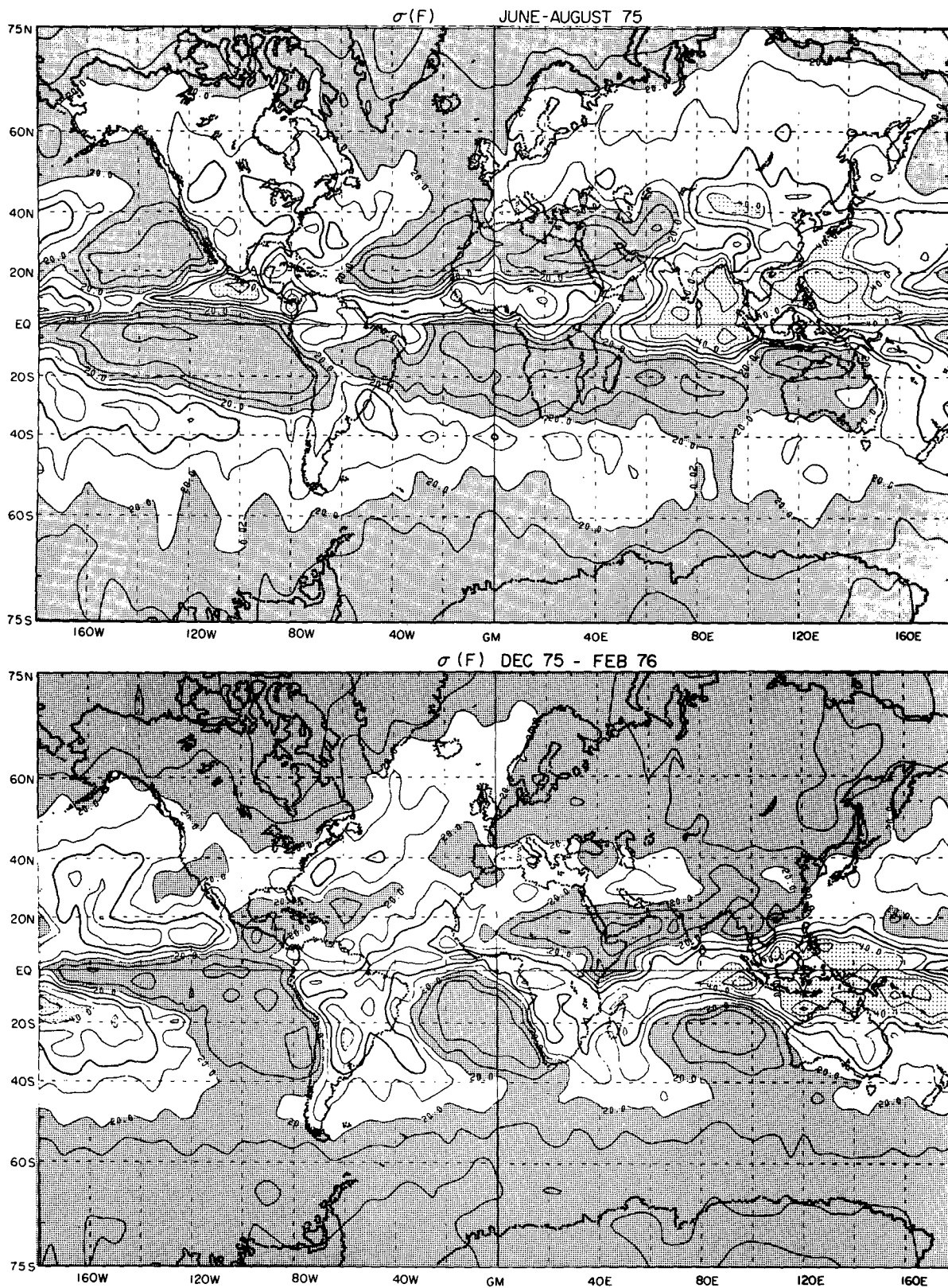


FIG. 4. Standard deviation of outgoing IR from day-to-day variations for two seasons. Contour interval is every  $5 W m^{-2}$  with values greater than  $40 W m^{-2}$  stippled and values less than  $20 W m^{-2}$  shaded.

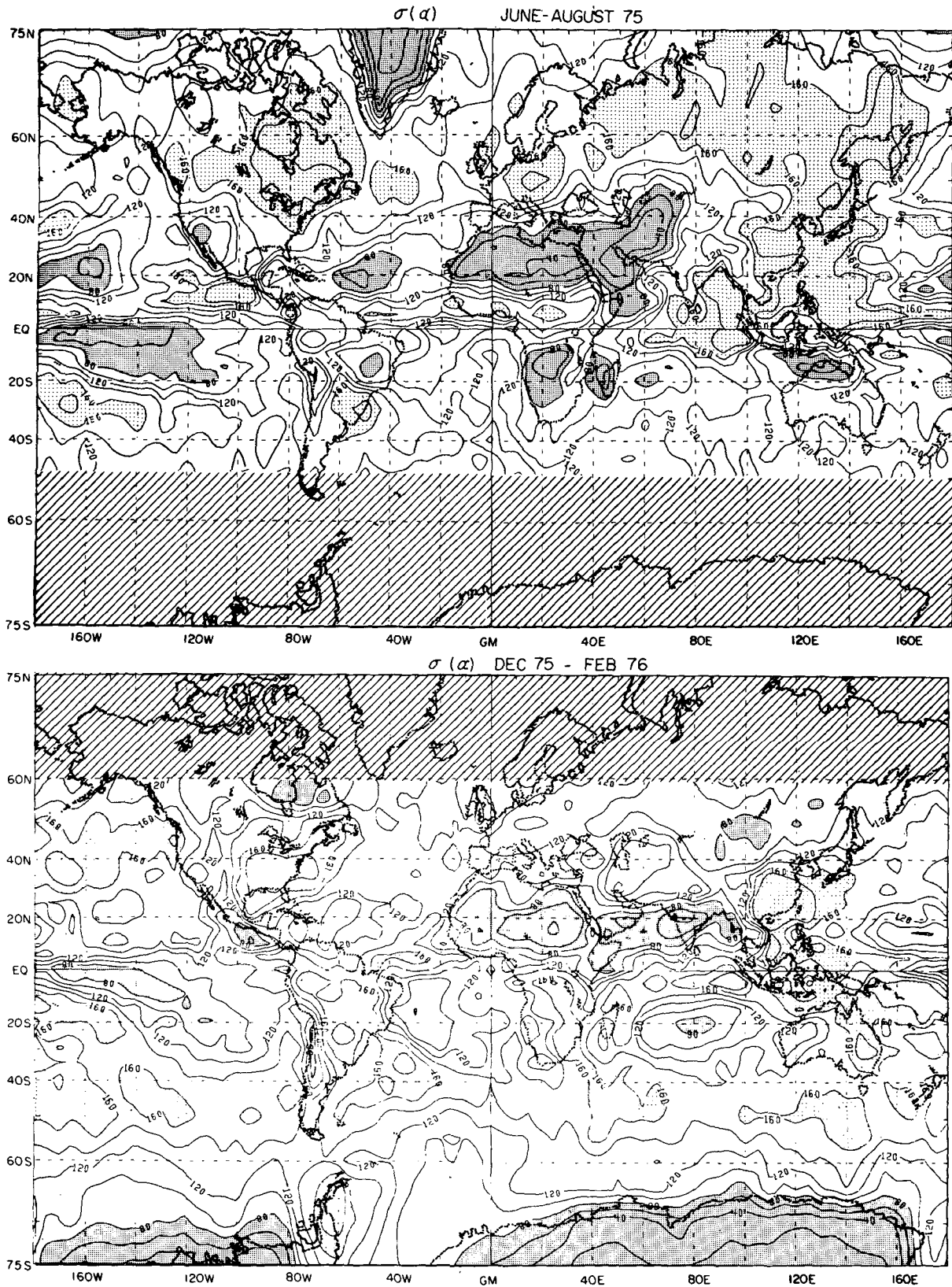


FIG. 5. Standard deviation of albedo in percent  $\times 10$  for two seasons. Contour interval is every 20 ( $2\% \times 10$ ) with values greater than 160 stippled and values less than 80 shaded.

from variations in cloudiness, and the resulting patterns of variability appear to be consistent with this interpretation. In this section we will look at the relationship between local changes in albedo and outgoing IR. Scatter diagrams of albedo versus outgoing IR for 15 locations are shown in Fig. 6. The solid lines in each of the 15 panels represents a linear fit to the approximately 90 data points. It can be seen that in most cases the data can be said to have a characteristic slope  $\partial F/\partial\alpha$  which is well represented by the line of regression. Scatter about the line of regression may be caused by fluctuations in the type of cloud and, the temperature or humidity in the field view. Even in those cases where there is more than one cloud type within the area of interest, such as in Figs. 6e, 6h and 6n, the regression line represents a reasonable compromise for the slope  $\partial F/\partial\alpha$ . Values of  $\partial F/\partial\alpha$  determined by linear least square regression have been calculated at each point of a  $5^\circ \times 5^\circ$  grid and plotted for two seasons in Fig. 7. These maps are similar in some respects to the maps of the standard deviation of outgoing IR in Fig. 4. The comparison of Figs. 4 and 7 emphasizes the central importance of regional variations in cloud height in controlling regional variations in  $\partial F/\partial\alpha$ . The value of  $\partial F/\partial\alpha$  is a very sensitive indicator of low-cloud regimes and reveals the extent and location of the well known stratus cloud regimes associated with the cold ocean current systems on the eastern sides of the Atlantic and Pacific Oceans. It also indicates a low-cloud regime in the Indian Ocean west of Australia and another over coastal China during winter. The low-cloud regime over eastern China results from the formation of low clouds and fog when low-level air from the warm ocean flows over the cool land surface during the passage of developing low pressure systems (Ramage, 1971). Positive values of  $\partial F/\partial\alpha$  are obtained over snow-covered regions in Canada and Russia during winter and over Greenland and Antarctica during summer.

##### 5. The net radiative effect of the current distribution of cloud

Because of their powerful influence on both absorbed solar radiation and outgoing terrestrial radiation, it has long been recognized that clouds could play an important role in determining the sensitivity of the earth's climate to perturbing influences. A logical simplification of the question of the role of cloudiness on climate sensitivity can be made by dividing it into two separate questions. First, how do various cloud types and cloud type distributions (in particular the current cloud type distribution) affect the net radiation balance of the earth? Second, how will the cloud type distribution and

fractional area coverage of cloud change as a result of changes in the climate? The first of these questions will be addressed here. The second question is a much more difficult one to answer at present, and is a particularly difficult one for which to find useful observational evidence.

Formally, we suppose that  $R_{\text{net}}(A_c, C, T, q, \alpha_s, \dots)$  is a function of a number of variables including  $C$ , which we take to represent a particular statistical distribution of cloud types according to cloud top temperature, albedo, thickness, overlap, etc., as well as the fractional area coverage of this distribution ( $A_c$ ), the temperature ( $T$ ) and humidity ( $q$ ) profile distributions, the surface albedo ( $\alpha_s$ ) and a number of other factors. In order to answer the first question regarding the net radiative effect of the current distribution of cloud, we wish to evaluate the partial derivative  $\partial R_{\text{net}}/\partial A_c$  ( $C, T, q, \alpha_s, \dots$  taken while holding constant all variables which control  $R_{\text{net}}$  except  $A_c$ ). Schneider (1972) made a theoretical estimate of the net effect of cloudiness on the radiation balance by assuming specific cloud properties. For cloud properties which he felt were appropriate for the earth, Schneider estimated that globally the albedo effect of clouds would be larger than the IR effect and that an increase in cloudiness would lead to a reduction in the net radiation balance. Specifically he obtained  $\partial R_{\text{net}}/\partial A_c = -58 \text{ W m}^{-2}$ .

Cess (1976) used a different approach to obtain an estimate of  $\partial R_{\text{net}}/\partial A_c = 2.6 \text{ W m}^{-2}$ , which would indicate that cloudiness changes have a very small effect on the net radiation balance. To obtain this estimate he first derived a linear empirical equation to predict outgoing IR from surface temperature ( $T_s$ ) and fractional coverage of cloud. The data used in the regression to obtain the coefficients of this equation were annually and zonally averaged observations of surface temperature, cloudiness and outgoing IR at  $10^\circ$  latitude intervals. Since Cess performs his regression between  $F$ ,  $A_c$  and  $T_s$  over latitudinal variations, his value of  $\partial R_{\text{net}}/\partial A_c$  is not obtained while holding other variables such as the statistical distribution of cloud properties  $C$ , surface temperature  $T_s$  and humidity  $q$  constant, and is therefore not a partial derivative in the true sense. If anything, the regression relationship and subsequent climate sensitivity analysis performed by Cess is a sort of climate change experiment. One can argue, however, that latitudinal variations are probably not an appropriate analog for climatic change, since the circulation regime changes with latitude as well as the surface temperature. A regression of the type performed by Cess places deep tropical convective cloud, midlatitude layer cloud associated with cyclonic storms, and arctic stratus together in the same regression for  $F$  versus  $A_c$  and  $T_s$ . Since the median cloud height and temperature

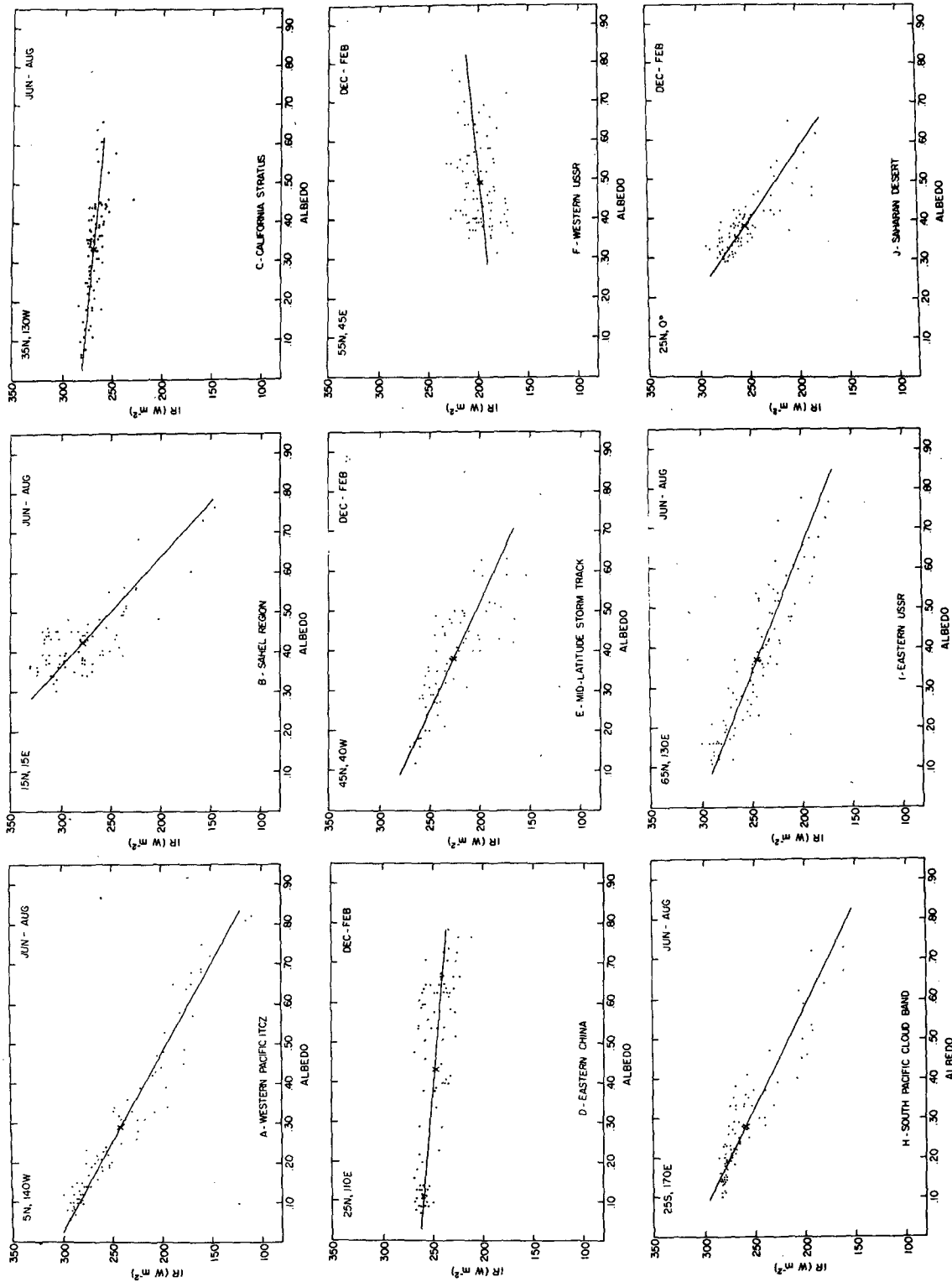


FIG. 6. Scatter diagrams of outgoing IR versus albedo for various geographical locations. The solid line represents a least squares fit to the 90 data points for the season of interest.

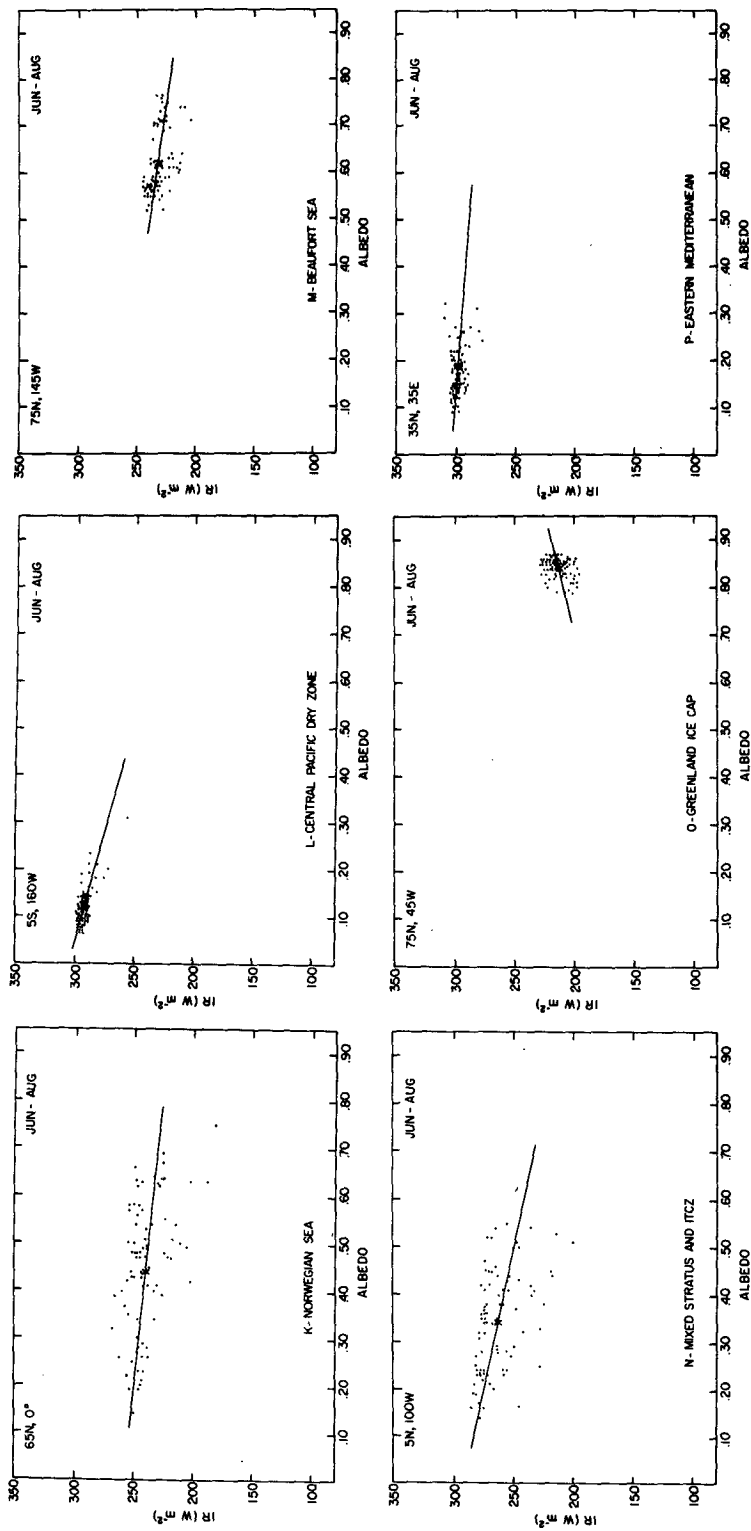


FIG. 6. Continued.

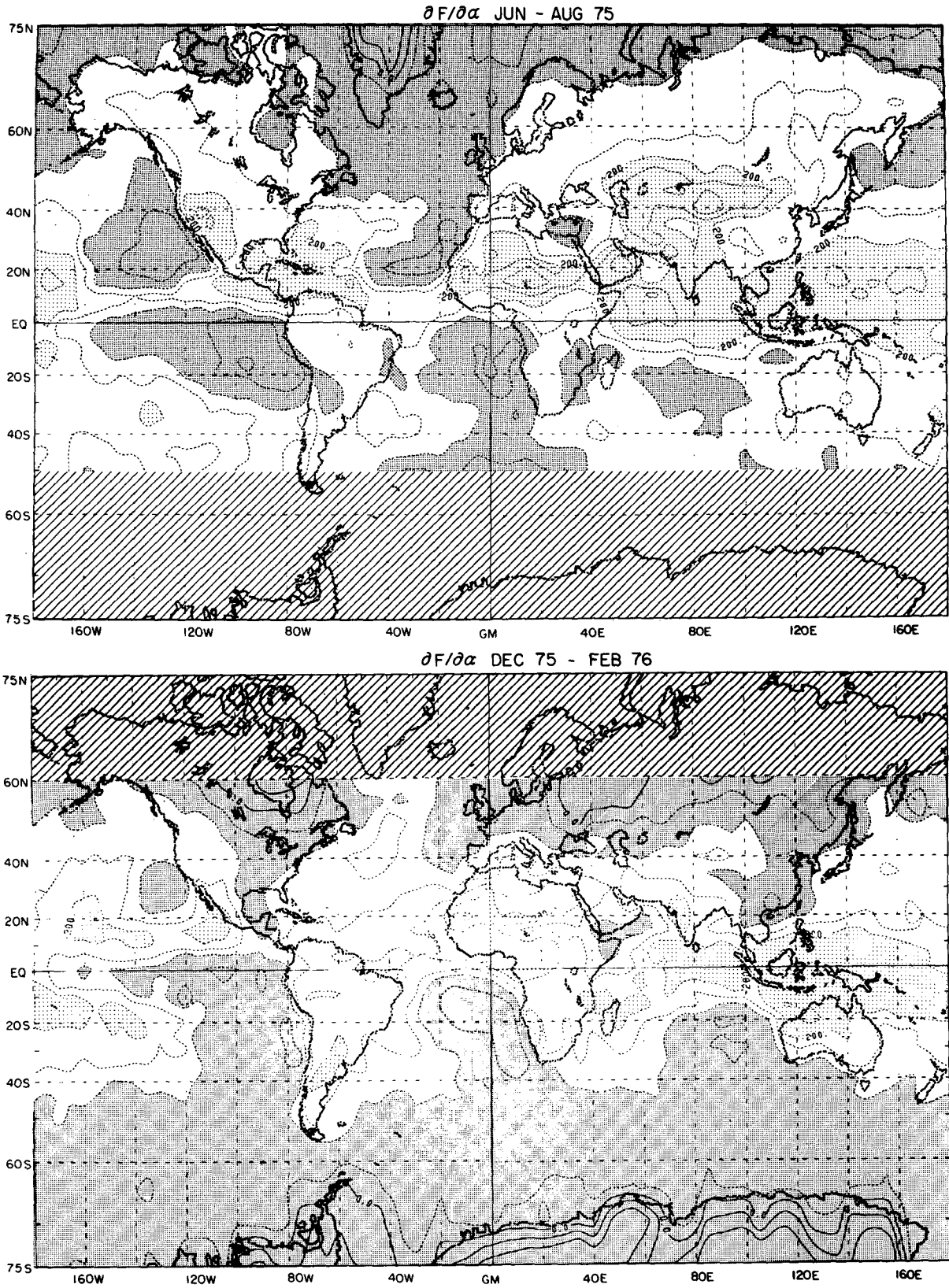


FIG. 7. Slope of outgoing IR versus albedo,  $\partial F/\partial \alpha$ , determined by linear regression. Contour interval is every  $50 \text{ W m}^{-2}$  with values less than  $-200 \text{ W m}^{-2}$  stippled and values greater than  $-100 \text{ W m}^{-2}$  shaded. Sparse albedo data are indicated by crosshatching.

contrast between cloud top and ground generally decreases with latitude as  $A_c$  increases and both  $T_s$  and  $F$  decrease, a regression over latitude can be expected to give rather large negative values for  $\partial F/\partial A_c$ , as indeed Cess found. An argument in support of this large value of  $\partial F/\partial A_c$  based upon hemispheric mean calculations has been presented by Cess and Ramanathan (1978).

Ellis (1978), rather than using latitudinal variations as an analog for climatic change, attempted to evaluate the net radiative effect of the present distribution of cloud by comparing outgoing IR and albedo for what were presumed to be cloudless skies with outgoing IR and albedo for average conditions. With auxiliary observations of the fractional area coverage of cloud, Ellis could then estimate  $\partial R_{net}/\partial A_c$  as

$$\frac{\partial R_{net}}{\partial A_c} \approx \frac{R_{net \text{ average}} - R_{net \text{ clear}}}{A_c}$$

Ellis estimated clear sky conditions as those under which the planetary albedo was near a minimum determined over a period of two weeks. The accuracy of his method depends critically on the accurate determination of this minimum and on the value of the fractional area coverage of cloud which was used. Using this method Ellis found that the present distribution of cloud is about twice as effective in reflecting solar radiation as in trapping IR and obtained a value of  $\partial R_{net}/\partial A_c = -35 \text{ W m}^{-2}$ . The approach used by Ellis appears to be an appropriate method for evaluating  $\partial R_{net}/\partial A_c$  while holding all variables except  $A_c$  fixed since it compares cloudy and clear conditions at a particular point and season.

Cess (1976) and Ellis (1978) obtained results which were determined for globally or zonally averaged conditions and were subject to a number of assumptions and uncertainties. In this section we will describe a method to determine the net radiative effect of cloud which uses a different set of assumptions. Furthermore, we will present our results in map form without spatial averaging. To derive the basis for our method we differentiate (1) with respect to  $A_c$  to obtain

$$\frac{\partial R_{net}}{\partial A_c} = -Q \frac{\partial \alpha}{\partial A_c} - \frac{\partial F}{\partial A_c}, \tag{2}$$

and factor the right-hand side with the result

$$\begin{aligned} \frac{\partial R_{net}}{\partial A_c} &= \left( \frac{-\partial F}{\partial A_c} \right) \left[ Q \frac{\partial \alpha}{\partial A_c} \left( \frac{\partial F}{\partial A_c} \right)^{-1} + 1 \right] \\ &= \left( -\frac{\partial F}{\partial A_c} \right) \left[ Q \frac{\partial \alpha}{\partial F} + 1 \right]. \end{aligned} \tag{3}$$

Here it is assumed that all derivatives are taken while holding  $C, T, q, \alpha_s$ , etc., constant and varying

only  $A_c$ . Note that  $\partial \alpha/\partial F$  as derived in (3) has the meaning of the change in albedo divided by the change in outgoing IR resulting from a change in  $A_c$  while holding all other variables constant. We now have an expression for  $\partial R_{net}/\partial A_c$  which is a product of two factors,  $-\partial F/\partial A_c$  and  $Q(\partial F/\partial \alpha)^{-1} + 1$ . The first of these,  $-\partial F/\partial A_c$ , depends primarily upon the difference between the surface and cloud top temperature and is known to be positive in most cases of interest. The second factor,  $Q(\partial F/\partial \alpha)^{-1} + 1$ , which we will hereafter call the cloud factor, is a dimensionless number which measures the relative importance of albedo and IR effects on the net radiation balance as follows:

$$\begin{aligned} \text{Cloud factor} &\equiv \left[ Q \left( \frac{\partial F}{\partial \alpha} \right)^{-1} + 1 \right] \\ &= \begin{cases} 1, & \text{IR effect only} \\ 0, & \text{IR and albedo effects} \\ & \text{cancel exactly} \\ -N, & \text{albedo effect is } N + 1 \\ & \text{times as large as IR effect.} \end{cases} \end{aligned}$$

The cloud factor can be much less than  $-1$ , in which case the interpretation is that the clouds present are much more effective in reflecting solar radiation than they are in reducing outgoing terrestrial radiation.

In using (3) to evaluate the net effect of clouds on the radiation balance we used the value of  $\partial F/\partial \alpha$  determined from linear regression described in the previous section. We assume that the value of  $\partial F/\partial \alpha$  derived at a particular point during a season results principally from changes in the fractional area coverage of cloud in the region of interest and not to any important extent from changes in the distribution of cloud properties at that point. We do not assume that  $F$  and  $\alpha$  are not affected by changes in humidity and temperature, but only that the variations imposed by changes in fractional area coverage of cloudiness are generally larger, possess more consistent correlations between  $F$  and  $\alpha$ , and therefore dominate in determining  $\partial F/\partial \alpha$ . This assumption is an excellent one in the tropics, but it may introduce greater uncertainty in midlatitudes in winter where variations in cloudiness are accompanied by substantial temperature and humidity fluctuations. While we formally assume that the statistical distribution of cloud properties does not change at a point during a season, the examples given in Fig. 6 suggest that a reasonable estimate for  $\partial F/\partial \alpha$  is obtained even where this assumption is violated and a mixed distribution of cloud types is present. The method which we have used to derive the cloud factor from observations should automatically take into account

any correlations between cloud top height and cloud albedo which may be present.

Although this method will not provide estimates of  $\partial F/\partial A_c$  and  $\partial R_{\text{net}}/\partial A_c$  without further assumptions, it does provide an estimate of the relative magnitudes of the changes in absorbed solar radiation and in outgoing IR which can be expected from a change in cloud coverage without a change in the distribution of cloud properties such as cloud top temperature and albedo. Moreover it provides this estimate from observations of  $F$  and  $\alpha$  only, does not require auxiliary measurements of  $A_c$ , and does not require the determination of the extrema of the  $\alpha$  or  $F$  distributions.

The values of the cloud factor obtained for two seasons are shown in map form in Fig. 8. The low-cloud regimes appear clearly as regions where the albedo effect is many times larger than the IR effect so that an increase in the extent or average  $A_c$  of the regions of low cloud would tend to reduce the net radiation and lead to a cooling of the earth. These regions are potentially very important because of the large area in the tropics which they encompass. Fig. 8 also indicates that the cloud factor is less than  $-1$  over more than half of the earth and is greater than zero only at high latitudes during winter and over the glaciated land masses of Greenland and Antarctica during summer. Even over those regions where we expect the highest cloud tops, the cloud factor is substantially negative, suggesting that even an increase in deep tropical convective cloud would tend to cool the earth. In high latitudes during winter where the available solar radiation is small (indicated by crosshatching) the value of the cloud factor should approach  $+1$ , since only the IR effect of cloud operates in the polar darkness.

It is useful to consider the effect on the evaluation of the cloud factor of the uncertainties in the proper value of  $\partial F/\partial \alpha$  resulting from the scatter about the regression lines shown in Fig. 6. Estimates of this uncertainty for nine geographical regions are shown in Fig. 9. The lettered crosses indicate the range in possible values of  $\partial F/\partial \alpha$  determined subjectively from examination of Fig. 6 and the range of  $Q$  resulting from the seasonal variation of insolation. Together  $\partial F/\partial \alpha$  and  $Q$  determine the cloud factor and lines of constant cloud factor are drawn on Fig. 9. The letters identifying the individual crosses correspond to the letters identifying particular locations in Fig. 6. The uncertainty of the estimate of  $\partial F/\partial \alpha$  and cloud factor is small for locations with homogeneous cloud populations (A,C,D,I) and large for regions with mixed populations (B,E,H,J). The letter G represents an estimate of the global average cloud factor and its uncertainty.

The maps of the cloud factor presented in Fig. 8 suggest that in the global mean the current distribution of cloud reduces the absorbed solar radiation more than it reduces the outgoing IR. The actual value of  $\partial R_{\text{net}}/\partial A_c$  cannot be deduced directly from Fig. 8, since the cloud factor must be multiplied by  $-\partial F/\partial A_c$  at each point before averaging, and we have not attempted to estimate  $\partial F/\partial A_c$  in this paper. In this regard it should be noted that the appearance of large negative values of the cloud factor over the regions of low cloud does not necessarily mean that their effect on  $R_{\text{net}}$  is larger than that of the regions of deep convection in the tropics, since the value of  $-\partial F/\partial A_c$  for the low-cloud regimes is probably considerably smaller than that of the high clouds in the convection zones. There are a number of ways in which  $\partial F/\partial A_c$  can be estimated from ERB data, but each involves additional assumptions. Ohring and Clapp (1980) have used a regression approach similar to the one employed here to obtain values of  $\partial F/\partial \alpha$  and  $\partial R_{\text{net}}/\partial \alpha$ , except that they used month-to-month rather than day-to-day variations. Their values for  $\partial F/\partial \alpha$  for the 18 points they investigated are similar to the values obtained for the same points in this study. They then obtained estimates of  $\partial F/\partial A_c$  and  $\partial R_{\text{net}}/\partial A_c$  by assuming values for the difference between cloudy and clear-sky albedos. Ohring and Clapp's estimates for the global values of  $\partial R_{\text{net}}/\partial A_c$  and  $\partial F/\partial A_c$  were about  $-65$  and  $-40 \text{ W m}^{-2}$ , respectively. These values indicate that the estimated albedo effect of cloudiness is nearly three times as large as the IR effect of cloudiness and corresponds to a global-mean cloud factor of about  $-2$ .

A graphical representation of some of the estimates of the net radiative effect of cloudiness is given in Fig. 10. Lines of constant cloud factor and constant  $\partial R_{\text{net}}/\partial A_c$  are plotted on a coordinate system whose axes are the difference in albedo between clear and cloudy conditions versus the difference in outgoing IR for the same two conditions. The letters indicate the estimates of Adem (1967) (A), Schneider (1972) (S), Cess (1976) (C), Ellis (1978) (E) and Ohring and Clapp (1980) (O). The heavy triangle encloses our estimate for the reasonable limits of uncertainty. The triangle is bounded by an upper limit on the globally averaged albedo contrast between clear and cloudy conditions of  $0.45$ , and upper bound on the outgoing IR contrast of  $-40 \text{ W m}^{-2}$ , and an upper bound on the cloud factor of about  $-0.9$ . These limitations still admit a wide range of possible values of  $\partial R_{\text{net}}/\partial A_c$  from about  $-35$  to  $-100 \text{ W m}^{-2}$  but they do suggest that  $\partial R_{\text{net}}/\partial A_c$  is substantially negative and that an increase in the fractional area coverage of the present distribution of cloud types

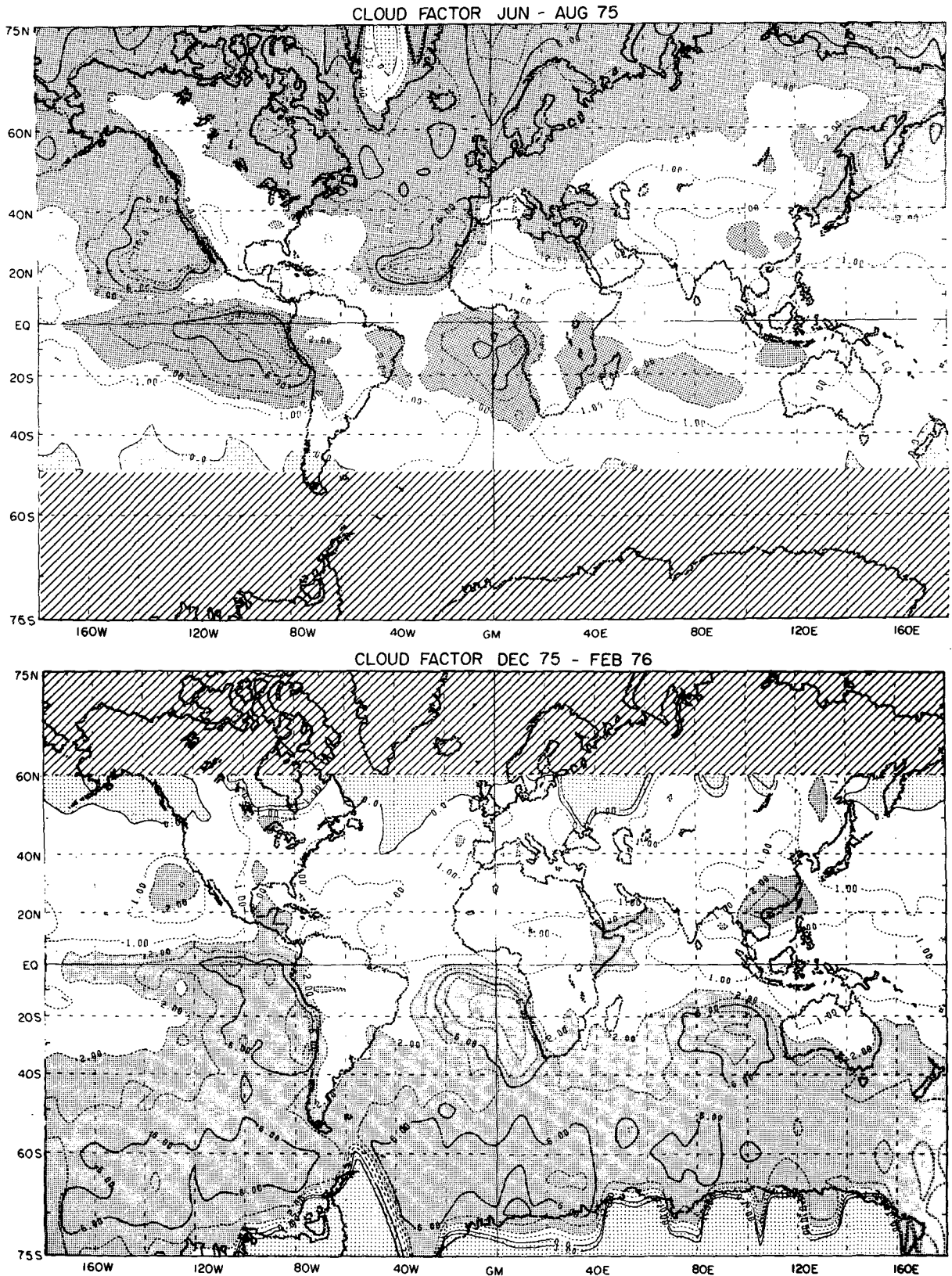


FIG. 8. Cloud factor  $[Q(\partial F/\partial \alpha)^{-1} + 1]$  explained in the text for two seasons. Contour interval is one from +1.0 to -2.0 and two from -2.0 to -10.0. Values greater than zero are stippled and values less than -2.0 are shaded.

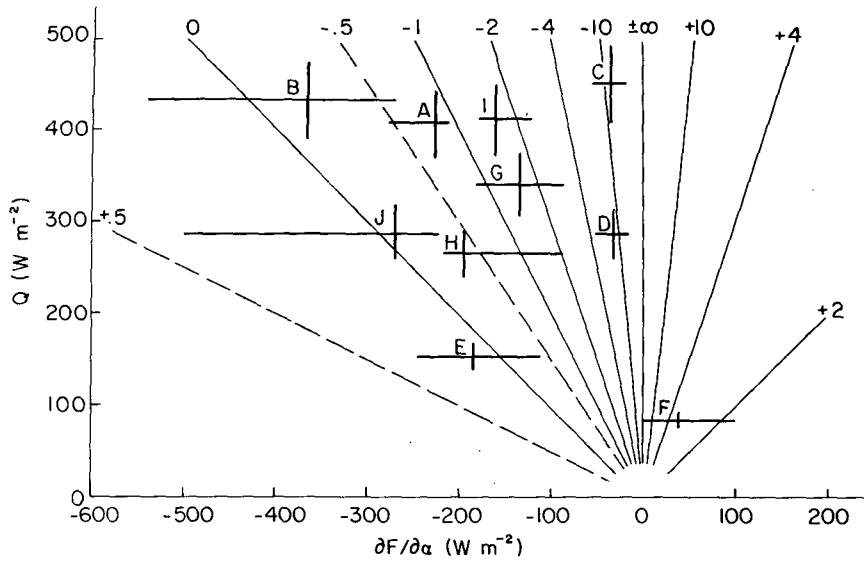


FIG. 9. Estimated range of uncertainty of the cloud factor  $[Q(\partial F/\partial \alpha)^{-1} + 1]$  for various regions identified by the letters in Fig. 6. Sloping lines are lines of constant cloud factor. The horizontal and vertical lines identified by the letter G are an estimate of the range of uncertainty of the global mean cloud factor.

would reduce  $R_{net}$  and lead to a cooling of the earth. It is perhaps not appropriate to include the result of Cess (1976) in Fig. 9, since, as discussed earlier, it is not really a measure of the net radia-

tive effect of the current global distribution of cloud. It is interesting that the estimates of Adem, Schneider and Ellis, while representing a range of values of  $\partial R_{net}/\partial A_c$ , all yield a similar value of the

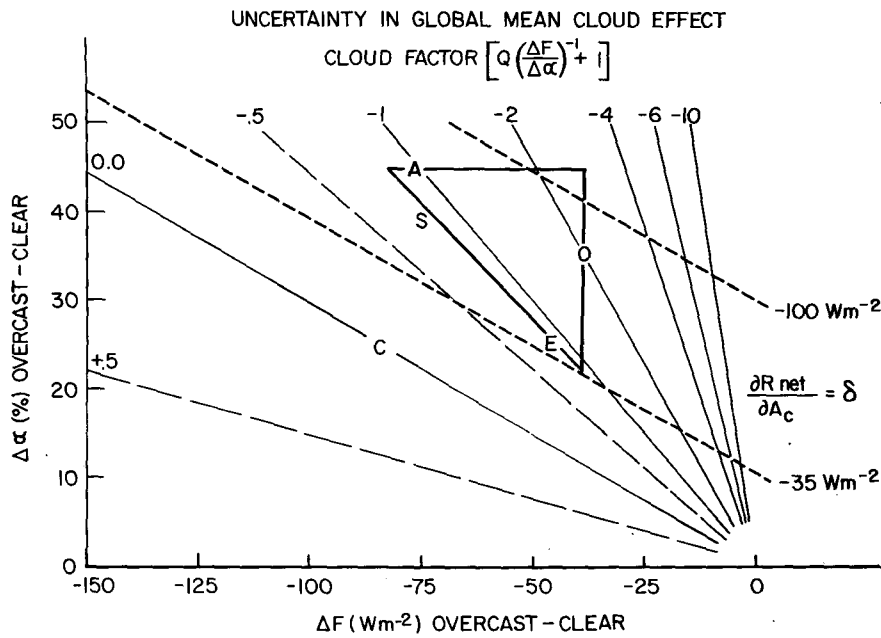


FIG. 10. Graph with coordinates of overcast-clear albedo contrast versus overcast-clear outgoing IR contrast. Radial set of light lines are lines of constant cloud factor with values of cloud factor indicated across the top and to the left of the figure. Heavy dashed lines are lines of constant  $\partial R_{net}/\partial A_c$ . The heavy triangle encloses the range of probable global mean values for the earth. The letters represent previous estimates of the effect of cloud amount change on the net radiation budget. A, Adem (1967); S, Schneider (1972); C, Cess (1976); E, Ellis (1978); O, Ohring and Clapp (1980).

cloud factor of about  $-1$ . They therefore agree as to the relative importance of the albedo and IR effects of clouds on the net radiation balance, but disagree slightly concerning the absolute magnitude of the net effect.

## 6. Discussion

In addition to the familiar maps of average outgoing IR, albedo and net radiation, maps of the standard deviation of outgoing IR and albedo and maps of the linear least square relation between outgoing IR and albedo,  $\partial F/\partial\alpha$ , have been presented. These last three statistics show distinctive geographical patterns which provide additional insight which is not easily gained from the mean values alone. These geographical patterns can be related to known features of the general circulation such as the precipitation zones, subsidence zones and deserts of the tropics, and the storm tracks of middle latitudes.

Since outgoing IR and albedo are such fundamentally important climatic variables, it is natural to compare the observed geographical patterns of these variables with patterns produced by numerical general circulation models. It is suggested here that not only the mean values be compared, but also the variability of albedo and outgoing IR and their cross correlation, as represented, for example by  $\partial F/\partial\alpha$ . This would be particularly appropriate for general circulation models which predict cloudiness, since through comparison of observed and model produced ERB statistics it should be possible to gain considerable insight into the usefulness of these cloud prediction schemes for modeling the sensitivity of climate.

The results presented in Section 5 indicate that the current distribution of cloud reduces absorbed solar radiation more effectively than it reduces outgoing IR. This result, while consistent with the result obtained by Ellis (1978) with an independent data set, probably should be verified with future observations which have more complete coverage of the solar and terrestrial emission spectra and which fully account for diurnal variations. The geographical variability of the cloud feedback factor shown in Fig. 8 suggest relationships between circulation patterns and the type of cloud present. The subsidence zones are generally associated with low clouds which effectively reduce the net radiation, while the precipitation zones are associated with tall clouds for which the albedo and IR effects are more nearly in balance. Second-moment statistics such as the cloud factor and  $\partial F/\partial\alpha$  should be very sensitive indicators of changes in the circulation and cloudiness patterns in the tropics, especially. For example, it is known that large shifts in the boundaries of the precipitation and subsidence

zones are associated with El Niño events in the equatorial Pacific. Further studies of several years of second-moment ERB statistics may provide needed insight into the relation between circulation changes and cloudiness changes in the tropics.

*Acknowledgments.* The authors would like to thank J. M. Wallace for reading the manuscript. This research was supported by the Climate Dynamics Program, Climate Dynamics Research Section, Atmospheric Sciences Division, National Science Foundation under Grant 78-07369.

## REFERENCES

- Adem, J., 1967: On the relations between outgoing longwave radiation, albedo, and cloudiness. *Mon. Wea. Rev.*, **95**, 257–260.
- Arakawa, H., 1969: *Climates of Northern and Eastern Asia. World Survey of Climatology*, Vol. 8, Elsevier, 450 pp.
- Cess, R. D., 1976: Climate Change: An appraisal of atmospheric feedback mechanisms employing zonal climatology. *J. Atmos. Sci.*, **33**, 1831–1843.
- , and V. Ramanathan, 1978: Averaging of infrared cloud opacities for climate modeling. *J. Atmos. Sci.*, **35**, 919–922.
- Ellis, J. S., 1978: Cloudiness, the planetary radiation budget, and climate. Ph.D. thesis, Colorado State University, 129 pp.
- Erickson, C. O., and J. S. Winston, 1972: Tropical storm, mid-latitude cloud band connections and the autumnal buildup of the planetary circulation. *J. Appl. Meteor.*, **11**, 23–36.
- Grose, W. L., and B. J. Hoskins, 1979: On the influence of orography on large-scale atmospheric flow. *J. Atmos. Sci.*, **36**, 223–234.
- Gruber, A., and J. S. Winston, 1978: Earth-atmosphere radiative heating based on NOAA scanning radiometer measurements. *Bull. Amer. Meteor. Soc.*, **59**, 1570–1573.
- Jacobowitz, H., W. L. Smith, H. B. Howell, F. W. Nagle, and J. R. Hickey, 1979: The first 18 months of planetary radiation budget measurements from the Nimbus 6 ERB experiment. *J. Atmos. Sci.*, **36**, 501–507.
- Lau, N.-C., 1979a: The structure and energetics of transient disturbances in the Northern Hemisphere wintertime circulation. *J. Atmos. Sci.*, **36**, 982–995.
- , 1979b: The observed structure of tropospheric stationary waves and the local balances of vorticity and heat. *J. Atmos. Sci.*, **36**, 996–1016.
- Manabe, S., and R. T. Wetherald, 1967: Thermal equilibrium of the atmosphere with a given distribution of relative humidity. *J. Atmos. Sci.*, **24**, 241–259.
- Ohring, G., and P. Clapp, 1980: The effect of changes in cloud amount on the net radiation at the top of the atmosphere. *J. Atmos. Sci.*, **37**, 447–454.
- Ramage, D. S., 1971: *Monsoon Meteorology*. Academic Press, New York, 296 pp.
- , and C. V. R. Raman, 1972: *Meteorological Atlas of the International Indian Ocean Expedition*. Govt. Printing Office, Washington, DC, 121 pp.
- Raschke, E., T. H. Vonder Haar, W. R. Bandeen and M. Pasternak, 1973: The annual radiation balance of the earth-atmosphere system during 1969–1970 from Nimbus 3 measurements. *J. Atmos. Sci.*, **30**, 341–364.
- Roberts, R. E., J. E. A. Selby and L. M. Biberman, 1976: Infrared continuum absorption by atmospheric water vapor in the 8–12  $\mu\text{m}$  window. *Appl. Opt.*, **15**, 2085.
- Schneider, S. H., 1972: Cloudiness as a global feedback

- mechanism: The effects of the radiation balance and surface temperature of variations in cloudiness. *J. Atmos. Sci.*, **29**, 1413-1422.
- Short, D. A. and J. M. Wallace, 1980: Satellite-inferred morning to evening cloudiness changes. *Mon. Wea. Rev.*, **108** (in press).
- Taubensee, R. E., 1976: Weather and circulation of December 1975. *Mon. Wea. Rev.*, **104**, 325-330.
- Vonder Haar, T., and V. Suomi, 1971: Measurements of the earth's radiation budget from satellites during a 5-year period. Part I: Extended time and space means. *J. Atmos. Sci.*, **28**, 305-314.
- Wagner, A. J., 1976: Weather and circulation of January 1976. *Mon. Wea. Rev.*, **104**, 491-498.
- Winston, J. S., 1967: Planetary scale characteristics of monthly mean long-wave radiation and albedo and some year to year variations. *Mon. Wea. Rev.*, **95**, 235-256.
- , 1969: Global distribution of cloudiness and radiation as measured from weather satellites. *World Survey of Climatology*, Vol. 4, D. F. Rex, Ed., Elsevier, 247-280.